Received May 24, 2021, accepted June 7, 2021, date of publication June 14, 2021, date of current version June 22, 2021.

Digital Object Identifier 10.1109/ACCESS.2021.3089424

Numerical Design and Investigation of Circularly Segmented Air Holes-Assisted Hollow-Core Terahertz Waveguide as Optical Chemical Sensor

M. HUSSAYEEN KHAN ANIK[1], S. M. RIAZUL ISLAM[2], (Member, IEEE), SHOVASIS KUMAR BISWAS[3], (Member, IEEE), M. IFAZ AHMAD ISTI[1], MOHONA DAS GUPTA[1], MD. JALIL PIRAN[2], (Senior Member, IEEE), KYUNG-SUP KWAK[4], (Life Senior Member, IEEE), AND HRITESHWAR TALUKDER[1], (Member, IEEE)

[1]Department of Electrical and Electronic Engineering, Shahjalal University of Science and Technology, Sylhet 3114, Bangladesh
[2]Department of Computer Science and Engineering, Sejong University, Seoul 05006, South Korea
[3]Department of Electrical and Electronic Engineering, Independent University, Bangladesh (IUB), Dhaka 1229, Bangladesh
[4]School of Information and Communication Engineering, Inha University, Incheon 22212, South Korea

Corresponding authors: Kyung-Sup Kwak (kskwak@inha.ac.kr) and Hriteshwar Talukder (hriteshwar-eee@sust.edu)

This work was supported in part by the National Research Foundation of Korea-Grant funded by the Korean Government (Ministry of Science) under Grant ICT-NRF-2020R1A2B5B02002478, and in part by the Shahjalal University of Science and Technology (SUST Research Centre), Bangladesh, under Project AS/2020/1/34.

M. Hussayeen Khan Anik, S. M. Riazul Islam, and Shovasis Kumar Biswas contributed equally to this work and co-first authors.

ABSTRACT In this paper,a polarization-maintaining single-mode rectangular-shaped hollow-core waveguide with four segmented air cladding in the terahertz (THz) regime is presented for detecting various toxic industrial chemicals. A new type of injection moldable cyclic olefin copolymer, commercially named as TOPAS is used as the base fiber material for its high optical transmission and high resistance to other chemicals. The finite element method with a perfectly matched layer as the boundary condition is employed for numerical explorations. The proposed sensor exhibits ultra-high relative sensitivity of 99.73% and ultra-low effective material loss of 0.007 cm^{-1} at 1.6 THz frequency for Toluene in y polarization. This sensor also evinces a high birefringence of 4.16×10^{-3} at 1.6 THz frequency. A maximum V parameter of 2.224 has been found at 2.2 THz which ensures the single-mode propagation of light. The sensor shows a very low confinement loss of 3.2×10^{-11} dB/m and a high numerical aperture of 0.3574 at 1.6 THz frequency for Hydrogen Sulfide. This paper also concentrates on other important design parameters such as bending loss, mode field radius, beam divergence and effective area for serviceability of the sensor in the THz region. This sensor can be a very good candidate for various chemical detection as well as other applications in the terahertz regime.

INDEX TERMS Bending loss, effective material loss, numerical aperture, relative sensitivity, terahertz, optical chemical sensor, waveguide.

I. INTRODUCTION

Electromagnetic (EM) wave propagation through a dielectric medium occurs via index guided or photonic bandgap mechanism. Recently, a lot of studies have been conducted on waveguides for the guidance of terahertz (THz) frequency of EM waves. This region of operation lies within the infrared to the microwave frequency bands, particularly 0.1-10 THz or 30 μm to 3 mm wavelength of light [1]. THz EM waves travel at a higher wavelength, which effectively distorts the propagating wave, causing unwanted phenomena, such as material absorptions losses and divergence of the beam waist. This has led to the vacuum or free space applications of the THz waves. But because of issues like alignment problems of the source and the detector and uncertain propagation losses, THz wave guidance has become a limited prospect to carry out its applications [2]. The multifarious applications of the THz regime found its way to biotechnology [3], analysis of ribonucleic acid and deoxyribonucleic acid [4], [5], THz imaging of cancer cells [6], security purposes [7], detection of research department explosives [8] and many more.

The associate editor coordinating the review of this manuscript and approving it for publication was Sukhdev Roy.

At present, researchers are focusing on the computational development of THz waveguides and running their numerical investigations. The most recent studies on THz waveguides have been carried out accordingly for terahertz guidance, broadband applications and sensing purposes. The main goal for the waveguides is to reduce the different loss mechanisms that the waveguides suffer generally, which include confinement losses, material absorption losses and bending losses. For sensing purposes, the most significant parameter is the relative sensitivity, which gives an idea of how well the THz guided EM wave interacts with the target analytes. As mentioned earlier, a calibrated index difference between the core and the cladding or a geometrically induced photonic bandgap can guide light through the waveguides. For this purpose, photonic crystal fibers (PCF) have found its immense usage in a diverse field of photonics. The unique existence of the periodic refractive index of such fibers can guide light by both the guiding mechanism. Previously, we have numerically developed PCFs which show enhanced optical properties in terms of broadband communications [9], [10]. PCFs working under the principle of surface plasmon resonance (SPR) have a dominant sensing response with analyte refractive index changes. We have modeled PCF-SPR based sensors that utilize the different guiding mechanisms for EM light interaction with analytes [11]. The study shows a satisfactory sensing response for analyte index alterations. However, the THz EM waves have greater wavelengths which cause the absorption loss mechanisms to impede the output response. The efficient functionality of THz waveguides depends on the tactical orientation of the geometric design. The recent studies of all THz waveguides have been conducted computationally to obtain the optical characteristic responses. A porous core circularly slotted PCF design has achieved high birefringence and low effective material or absorption loss (EML) of 0.07 cm^{-1}. Additionally, it shows a low bending loss of the order 10^{-9} dB/m in the operating THz regime [12]. Another novel diamond core PCF portrays losses close to the former [13]. Numerical investigations on PCFs for targeted analyte detection have been carried out recently for different proposed models. A rectangular-hollow core PCF for benzene, water and ethanol detection has achieved a good relative sensitivity (RS), with a maximum value of 89% for benzene. A most recent study in 2020, enunciates that 94.4% sensitivity can be achieved for bane chemical detection using a PCF model [14]. However, the fabrication of such a design is a critical issue as all rectangular airholes comprise the whole structure. The study has not focused on beam waist divergence, numerical aperture, spot size, mode field radius or effective area. The structure also has not been able to achieve any birefringence due to higher rotational symmetry. In another study, the authors have claimed their design to be an ultra-low loss PCF with an EML of 0.04 cm^{-1} at 1 THz frequency [15]. The PCF showed a confinement loss in the range 10^{-3}-10^{-6} within the operating frequency, which is not that low. Another chemical identifier THz PCF has been proposed with a Kagome structure which has attained a maximum RS = 85.7% [2]. From the numerical studies of THz waveguides for achieving high sensitivity, PCF arrangement with a periodic refractive index variation has been utilized mostly, with both solid core and porous core. Porous core where the analyte is introduced in the air holes in the core, shows higher RS, as more volume of the target analyte has the scope to interact with the guided light. However, the material absorption loss is significant as the guided light still has to pass through the background material. Having an eye on this issue, a THz waveguide has been designed with a decreased volume of the background material in the cladding [16]. The evanescent waves which travel with the core guided mode suffer less material absorption loss. The optical confinement of light is also higher.

This paper comes forwards with an efficient novel THz waveguide design with a rectangular channel in the core for the target analyte to be introduced. The higher percentage of the analyte in the channel formed in the core effectively reduces the absorption loss, increases the optical confinement, resulting in reduced confinement loss and most importantly, increases the relative sensitivity of the fiber for the target analytes. The strut which holds the analyte channel has been narrowed down near the core which decreases the loss mechanisms. The higher refractive index that gets formed in the core when the targeted toxic chemicals are introduced effectively guides the EM wave through the THz waveguide. The presence of toluene in a solution introduced in the kidney, liver or the nervous system significantly hinders the biological activities in the body. Ethylene glycol causes eye and respiratory tract irritations. Flammable compound hydrogen sulfide exposure causes frostbite. Hydrogen cyanide results in organ system failure. Di-chloro-fluoro-methane is a harmful chlorofluorocarbon gas. All these toxic substances can be sensed and analyzed using the proposed THz waveguide. The numerical investigation shows that the lattice design has an ultra-high RS of 99.73%. Very low confinement loss, material absorption loss and a good numerical aperture with single-mode behavior at the operating THz frequency make the sensor a prime candidate to be fabricated for sensing purposes. Also, this study focuses on the birefringence effect for the sensing analytes, as the framework for the design makes the analyte to form up an asymmetric core.

II. MODELLING AND NUMERICAL ANALYSIS

The cross-sectional 2D representation of our proposed sensor is depicted in Figure 1(a). The sensor has a rectangular-shaped hollow core with a height and width marked as H and W respectively. Four segmented air holes in a circular manner have been placed at the outer section of the sensor. Chemical is passed through the rectangular-shaped hollow core at the center. The whole design has been made in this way to maximize the interaction of light with chemicals and increase the relative sensitivity. The 3D extended view of our proposed sensor has been portrayed in Fig. 1(b). Cyclic olefin copolymers are the updated class of thermoplastics which can be used as the background material of the fiber.

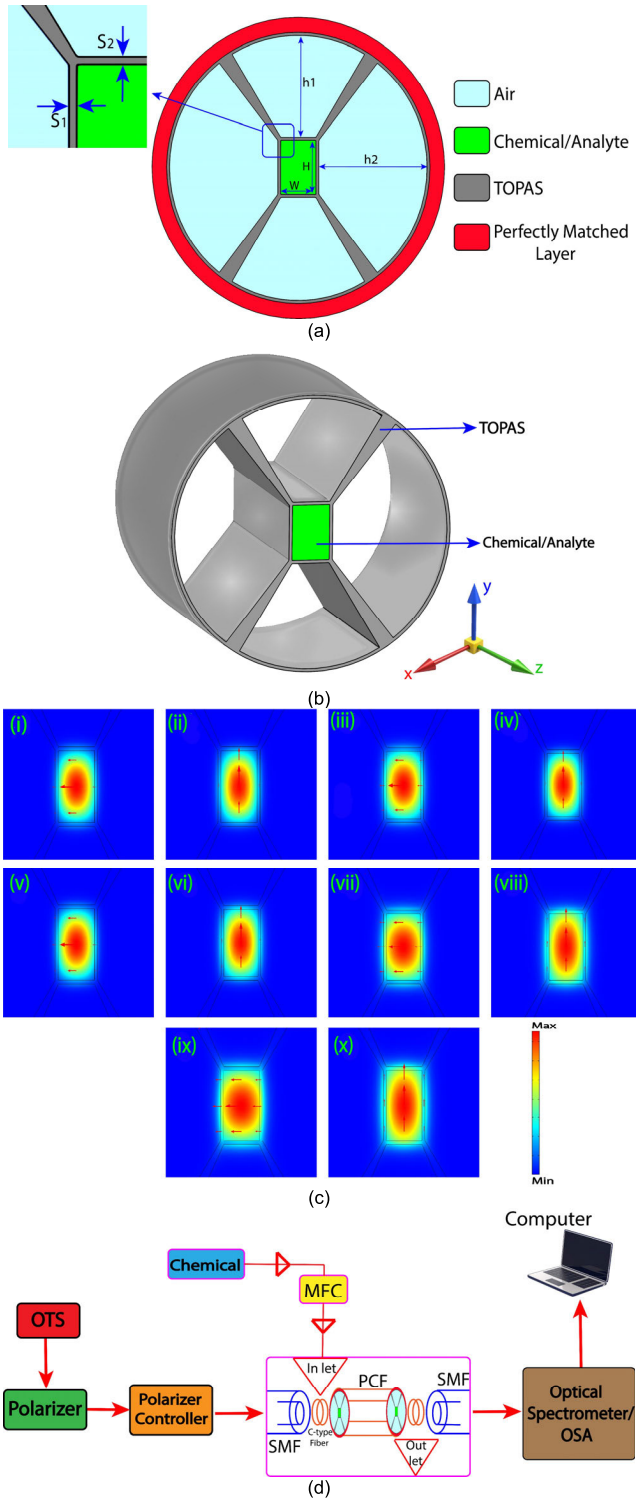

FIGURE 1. **Illustration of the proposed Sensor: (a) Geometry of the proposed design, (b) 3D extended view of the sensor, (c) Field profiles of the x and y polarization modes for the five toxic analytes, and (d) The experimental setup.**

These polymers have many attractive optical properties such as low absorption loss, low moisture uptake, high optical transmission, large Abbe number and chemical resistance. There are many types of polymer materials available just as polymethylmethacrylate (PMMA), Apel, Arton, Zeonex, Teflon and most recently Topas. PMMA and Teflon are not selected as background material of the fiber due to their higher moisture uptake, higher absorption loss and lower heat deflection than Topas. Zeonex is also not selected because it has a lower glass transition temperature than Topas. For fabrication feasibility, a high glass transition temperature is always required. However, Topas has almost a hundred times lower bulk material loss than PMMA with a very high optical transmission. Topas also has a constant index of refraction ($n = 1.53$) in the terahertz regime [15]. Considering all these facts, we have selected Topas as the base fiber material of our sensor.

Air holes have covered the maximum area of the sensor to reduce the effective material loss. Rectangular shaped hollow core with a large difference between the lengths of height and width helps to increase the birefringence of the sensor by making the core asymmetric. The porosity of the core is calculated as the ratio of the rectangular hollow core area and the total core area. A total of four segments of air cladding have been found with two different heights marked as $h1$ and $h2$. Ideal parameters found after proper investigations are $H = 360.8\ \mu m$, $W = 240.6\ \mu m$, $h1 = 680\ \mu m$ and $h2 = 740\ \mu m$. The TOPAS widths around the analyte channel are marked as S_1 and S_2 which is depicted in Fig. 1(a). The values of S_1 and S_2 are of 19.8μm and 19.6μm respectively. Total fiber radius is $1000\ \mu m$ with a non-physical perfectly matched layer (PML) that has been taken as a boundary condition. The thickness of the PML is kept at $100\ \mu m$ which is 10% of the whole fiber radius. PML absorbs unwanted radiation and eliminates environmental effects. The practical consciousness of our proposed sensor is manageable as there are existing technologies to fabricate the structure. For the rectangular-shaped hollow core, the excursion and 3D printing techniques can be applied [17]. Kagome structure has been proposed which is supported by a 3D printing mechanism [2]. Rectangular slotted airholes have been fabricated with extensive analysis previously, which can support the strut framework [18]. The extrusion technique used along with a stainless steel based or 3D printed extrusion die can easily realize the proposed sensor. For cleaving the porous fiber, focused ion beam milling is very effective. The orthogonal x and y polarized fundamental modes for the five different toxic analytes have been evaluated in Fig. 1(c). The structural circular asymmetry induced the two orthogonal modes. As the waveguide exhibits single mode behavior, the field profile of the fundamental modes remains almost the same.

For numerical investigations and optical portrayal of our sensor, the finite element method-based simulation tool Comsol Multiphysics is employed. To understand the sensing performance of a PCF sensor, various guiding properties should be discussed. One of the most important guiding properties of a PCF based sensor is relative sensitivity. It ensures the sensing capacity of a PCF sensor. Relative sensitivity measures the amount of interaction between the propagated light

and the chemical we have used as the analyte. Higher relative sensitivity means higher interaction between light and the chemical which is desirable for sensing perspective. It is denoted as r and can be determined as follows [19]:

$$r = \frac{n_s}{Re(n_{eff})}P, \tag{1}$$

where n_s is the refractive index of the chemical that is to be detected and $Re(n_{eff})$ is the real part of the effective mode index. P represents the percentage of interaction between the light and the chemical which is also called power fraction. P can be calculated as follows [19]:

$$P = \frac{\int_{analyte} Re\left(E_x H_y - H_x E_y\right) dxdy}{\int_{total} Re\left(E_x H_y - H_x E_y\right) dxdy} \times 100, \tag{2}$$

where E_x, E_y and H_x, H_y are the transverse electric and magnetic fields of the guided mode respectively.

Confinement loss is one of the limiting factors of a PCF sensor for sensing efficiency. Confinement loss happens due to the leaky nature of the mode. It determines the leakage of light while propagation and restricts the length of the fiber. Confinement loss can be determined by the imaginary part of the effective mode index as follows [20]:

$$L_c = 8.686 \times \frac{2\pi f}{c} Im\left[n_{eff}\right] \left(\frac{dB}{m}\right), \tag{3}$$

where f is the frequency of the light, $Im[n_{eff}]$ is the imaginary part of the effective mode index and c is the speed of light in free space.

Birefringence is another critical optical property of PCFs. It occurs due to the asymmetric shape of the hollow core. High birefringence is always desirable for polarization-maintaining fiber. The variation between the two orthogonal polarization creates birefringence. It can be calculated by the following equation [16]:

$$B = \left|n_{eff}^x - n_{eff}^y\right|, \tag{4}$$

where n_{eff}^x and n_{eff}^y are the effective mode indices of x and y-polarizations respectively.

All the polymers used as background material of the fiber have an absorption loss in high frequency. This absorbance is named as the EML. This kind of loss should be reduced as much as possible for increasing the sensing performance. This is an unavoidable loss but, selecting the proper geometric structure of the fiber as well as choosing suitable polymer EML can be minimized. Air holes have been placed in our sensor in such a way that they cover the maximum area of the fiber. We have intentionally reduced the background material area to minimize the EML. The EML specifies the total amount of electric field that is absorbed by the background material as a form of energy. The EML can be determined by the following equation [20]:

$$\alpha_{eff}\left[cm^{-1}\right] = \sqrt{\frac{\epsilon_0}{\mu_0}} \left(\frac{\int_{mat} n_{mat} |E|^2 \alpha_{mat} dA}{\left|\int_{all} S_z dA\right|}\right), \tag{5}$$

where α_{mat} and n_{mat} are the absorption loss and refractive index of Topas respectively. ϵ_0 and μ_0 indicate the relative permittivity and permeability of free space respectively. E is the electric field component and S_z denotes the z component of the poynting vector. S_z can be distinguished as follows [20]:

$$S_z = \frac{1}{2}\left(E \times H^*\right), \tag{6}$$

where H^* is the complex conjugate of the magnetic field.

The numerical aperture (NA) is another important optical property that measures angular acceptance of the incoming light into the fiber. A high value of NA will be satisfactory for a PCF sensor as it allows a good angular acceptance of light. NA is usually of the order of 0.1 for a single-mode fiber. Numerical aperture can be determined as follows [20]:

$$NA = \frac{1}{\sqrt{1 + \frac{\pi A_{eff} f^2}{c^2}}}, \tag{7}$$

where A_{eff} is the effective area. Effective area is a quantitative measurement of the area where the propagated light constructively covers in the transverse dimension. Effective area can be calculated by the following equation [9]:

$$A_{eff} = \frac{\left(\iint |E(x,y)|^2 dxdy\right)^2}{\iint |E(x,y)|^4 dxdy}, \tag{8}$$

where E is the electric field distribution.

V parameter is another dimensionless frequency parameter that ensures the number of modes of a PCF. To understand whether a PCF is single-mode or multimode, V parameter is a crucial guided property. It can be determined as follows [20]:

$$V = \frac{2\pi af}{c} \times NA, \tag{9}$$

where V is the V parameter. NA is the numerical aperture, where NA is the square root of the difference of the squares of the refractive index of the core and the cladding and a is the radius of the fiber core. As we have a rectangular-shaped hollow core at the center of the fiber, the equivalent value of the core radius is calculated using the area formula of a circle and a rectangle. Note that for V values below 2.405 usually support only one type of mode for propagation at a time per polarization direction.

In the context of splice loss, mode field radius (MFR) is an important optical property. Mode field radius is the transverse extent of the electric field distribution of a mode. For sensing standpoint, it is usually required to connect the PCF to a single-mode fiber (SMF) with a connector or fusion splicer. Optical power loss occurs at the joining or splicing point between the PCF and SMF. This loss should be minimized to increase the sensing efficiency and performance. MFR is one of the most crucial intrinsic parameters for splice loss. Higher splice loss can be noticed for a higher difference between the MFR of the PCF sensor and the MFR of the single-mode fiber. So, we need to know the mode field radius of our proposed sensor to deliver an idea for reducing the splice loss by making an SMF that has the mode field radius near

to our PCF sensor while establishing the connection. Mode field radius can be determined using Marcuse's equation as follows [21]:

$$W_{eff} = a\left(0.65 + \frac{1.619}{V^{\frac{3}{2}}} + \frac{2.879}{V^6}\right), \tag{10}$$

where W_{eff} is the mode field radius, a is the core radius and V is the V-parameter. This equation is accurate for the V values above *1*.

Beam divergence is closely related to the mode field radius of the sensor. Beam divergence is the measurement for how quickly a beam can expand far from its beam waist. It can also be defined as the derivative of the beam radius with respect to the centroidal position. A high beam divergence indicates less ability to focus a beam on a very small spot. Beam divergence can be calculated as follows [21]:

$$Beam\ divergence\left(\theta_{degree}\right) = \tan^{-1}\left(\frac{c}{\pi f W_{eff}}\right) \times \left(\frac{180^\circ}{\pi}\right), \tag{11}$$

where θ_{degree} is the angle of beam divergence in degree unit and W_{eff} is mode field radius of the sensor.

Bending loss is another important loss parameter that can be occurred when the fiber is bent. For a good sensing accuracy, bend loss of fiber should be lessened as much as possible. It can be calculated by the following equation [22]:

$$n_{eq}(x, y) = n(x, y)\left(1 + \frac{x}{R}\right), \tag{12}$$

where $n_{eq}(x, y)$ is the adjusted index of refraction of the PCF, $n(x, y)$ is the actual index of refraction of the used material, R represents the bend radius and x denotes the distance between the bending point and the center of the fiber. After getting the adjusted refractive index of the used material, simulation can be concluded another time to get a new imaginary part of the effective mode index ($Im[n_{eff}]$). Bending loss now can be determined by the new $Im[n_{eff}]$ using the equation (3). This method is vastly known as the conformal transformation method, where the bent fiber is hypothetically replaced by its equivalent straight fiber.

III. RESULTS AND DISCUSSION

A. PERFORMANCE OF THE THZ WAVEGUIDE

The electric field profiles are depicted in the Fig. 1(c). Because of the rectangular core area, the structure induces higher rotational asymmetry. This causes the formation of orthogonal x and y polarization core modes. The field profiles for all the target analytes are shown in the figure. The core confinement appears to be identical for the analytes. For the practical realization of the sensor, an experimental framework is portrayed in Fig. 1(d). An optical tunable source (OTS) is required to pass the light through the waveguide to have the interaction with the chemicals. This source can be broadband or supercontinuum. This light is passed through a polarizer and a polarizer controller to have a linearly polarized light. This light then can enter into a single mode fiber. SMF provides the opportunity to receive the light and take it into the waveguide. On the other hand, there will be chemicals that are to be sensed which are required to pass through a mass flow controller (MFC). MFC secures and controls the flow of those chemicals and lets them enter into the in-let. As we have an internal analyte flow channel in the core region of the waveguide, we need a C-type fiber. C-type fiber serves as a gas/chemical inlet and helps analyte to flow into the core channel of the PCF. Another C-type fiber is needed to serve as an outlet and extract out the analyte from the PCF. Then we will have another SMF that can receive the light from the THz waveguide after interacting with the chemicals and pass it through an optical spectrometer or optical spectrum analyzer (OSA). OSA can be utilized to sense the waveforms via computer. The quintessential target of this sensor is to attain maximum relative sensitivity. Relative sensitivity defines the extent to which the incident light interacts with the analytes. Fig. 2 demonstrates the variation of the relative sensitivity as a function of frequency for five different analytes. The analytes are Toluene ($n = 1.4747$), Ethylene glycol ($n = 1.427$), Hydrogen sulfide ($n = 1.3682$), Dichlorofluoromethane ($n = 1.285$), and Hydrogen cyanide ($n = 1.2675$). Here, n represents the refractive index of the respective chemicals. This figure exhibits that the relative sensitivity increases with an increase in frequency for all chemicals up to 1.6 THz. The power fraction continues to increase for all the chemicals from 1.2 THz to 1.6 THz because of the steady increment of the light confinement in the hollow core region. As a result, relative sensitivity also increases up to 1.6 THz. It is noticeable that the sensitivity lines for all the chemicals become almost parallel to the x-axis after 1.8 THz because of the balance between n_{eff} of the chemicals and power fraction. n_{eff} ceaselessly increases and power fraction steadily increases creating a balance between them resulting in straight sensitivity lines parallel to the x-axis after 1.8 THz for all chemicals. For hydrogen cyanide, as we go on increasing the frequency after 1.8 THz light internment and intensity slightly decrease which reduces power fraction as well as relative sensitivity. However, the

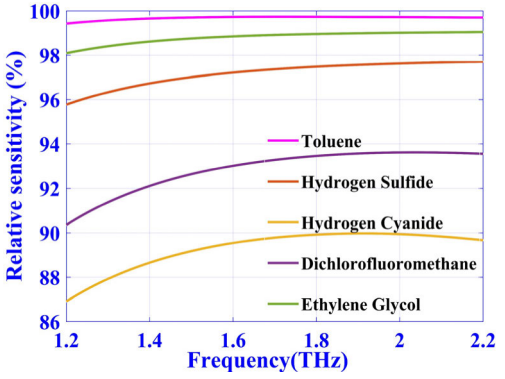

FIGURE 2. Relative sensitivity as a function of frequency for the target analytes.

concerned figure shows ultra-high relative sensitivities of 99.73%, 98.85%, 97.22%, 93.02%, and 89.56% for Toluene, Ethylene glycol, Hydrogen sulfide, Dichlorofluoromethane, and Hydrogen cyanide respectively at 1.6 THz which is better than all of the recently published papers. As the RS is directly proportional to the refractive index of the analyte, it appears to be the highest for toluene. Fig. 3(a) focuses on the effective index plotting with respect to the frequency alterations. It is evident from the figure that the effective mode indices for all the chemicals have a positive slope.

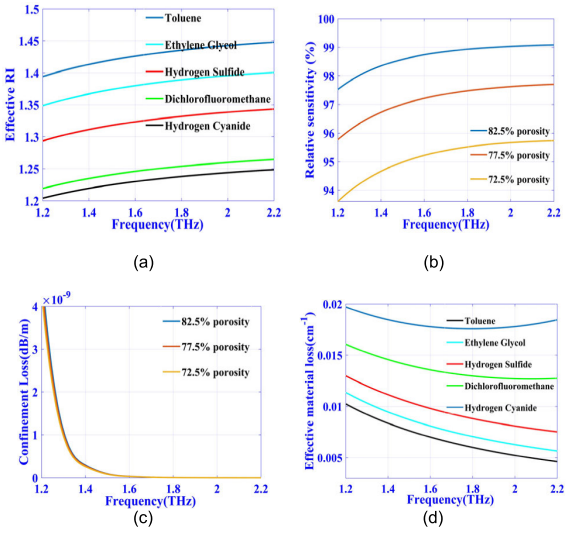

FIGURE 3. Illustration of optical characteristics of the proposed sensor: (a) Effective mode index for the corresponding analytes (b) Relative sensitivity response with variations of porosity for H_2S (c) Confinement loss for H_2S with variation of porosity (d) EML for all chemicals.

Fig. 3(b) indicates the relative sensitivity of H_2S with the increments in frequency for different porosities. Porosity is calculated as the ratio of the rectangular hollow core area and the total core area of the sensor. A higher porosity means a higher area of the rectangular hollow core, where the analyte is introduced. From the figure, it is revealed that high porosity increases the relative sensitivity which is rational as more of light will be able to interact with the chemical. In another sense, by increasing the porosity we can effectively reduce the area of the background material which creates a reduction in the absorption loss resulting in an increment in the relative sensitivity by offering more of the EM wave to interact with the target analyte in the hollow core region. When the porosity is reduced, it is observed from the figure that the relative sensitivity also reduces. By decreasing the hollow core area, we decrease the interaction between light and the analyte which lessens the relative sensitivity. The figure exhibits relative sensitivity of 98.74%, 97.22% and 95.22% for the porosities of 82.5%, 77.5% and 72.5% respectively at 1.6 THz. It is evident that the porosity has a very good impact on the sensitivity as it directly enhances the effective interaction between the propagated light and the chemicals in the hollow core.

B. LOSS MECHANISMS

Background materials experience different types of losses in terahertz band regime such as bending loss, confinement loss, effective material loss during transmission. The index difference between the core and the cladding induces an energy barrier for which photon confinement in the core is ensured. However, due to the tunneling effect, photons escape from the core to the cladding as evanescent waves. The higher is the penetration of the evanescent waves into the cladding, the higher will be the propagation loss of the core guided mode. Confinement loss can be curtailed by the appropriate design of PCF. The magnitude of the confinement loss is desired to be as small as possible because the light is expected to be confined in the core area of PCF without any loss. Fig. 3(c) demonstrates the variation of the confinement loss with frequency using Hydrogen sulfide as analyte for different porosities. More light confinement in the core results in low confinement loss. From 1.2-1.4 THz there exists a smaller value of confinement loss but after crossing 1.6 THz confinement loss becomes very negligible which is visualized in Fig. 3(c). However, the confinement loss of around 3.2×10^{-11}dB/m is found at 1.6 THz for all the porosities which is very low. The EML in the THz range for the five chemicals have been depicted in Fig. 3(d). Except Hydrogen Cyanide, the rest of the analytes have a decreasing slope with the increment of the frequency. It is observable from the figure that with the increase of the refractive index, the EML curve decreases significantly in the 10^{-2} range.

Fig. 4(a) represents the variation of the bending loss of the proposed sensor with frequency for different bending radius using Ethylene glycol as analyte. Bending loss is considered as an additional propagation loss caused by energy losses from core modes to the radiation modes when fibers are bent. It can be inferred from the figure that bending loss decreases with an increased bending radius because the curvature of fiber increases when the bending radius decreases. This causes the energy from the evanescent wave to be lost as radiation which distorts the core mode and the guided mode becomes lossy. This bending of the fiber causes the shifting of the fundamental mode field towards the cladding. In this case, after crossing 1.6 THz bending loss becomes negligible which is suitable for sensing applications. It is found from the figure that the bending losses are of 1.026×10^{-11} dB/m, 2.61×10^{-12} dB/m and 1.101×10^{-12} dB/m at 1.6 THz for bending radiuses of 2 cm, 2.5 cm and 3 cm respectively. It is clear from these data that bending loss increases with the decrement of the bending radius. The variation of the EML with frequency by varying porosity for hydrogen sulfide is elucidated in Fig. 4(b). As seen from the figure, the EML decreases with the increase of porosity. This is because the increase in porosity increases the area of the analyte, thereby decreasing the area of the background material. This results in the reduction of absorption loss by the background material which in turn reduces the EML. The figure exhibits that the EMLs of the background material are of 0.006703 cm^{-1},

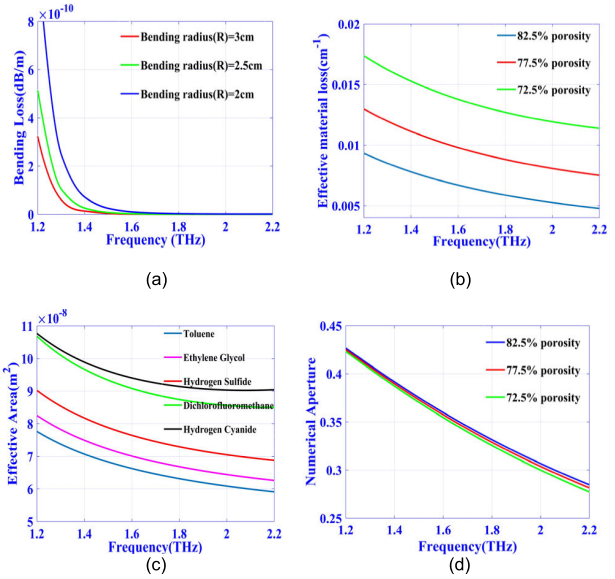

FIGURE 4. Illustration of optical characteristics of the proposed sensor: (a) bending loss for Ethylene glycol (b) Effective material loss (EML) with variation of porosities for H_2S (c) Effective area for all chemicals and (d) Numerical aperture with variation of porosities for H_2S.

0.009806 cm^{-1} and 0.01379 cm^{-1} at 1.6 THz for different porosities of 82.5%, 77.5% and 72.5% respectively. Fig. 4(c) shows the effective area of the proposed PCF design with the variation of frequency which indicates that the effective area of different materials is reduced with high frequency because of the strongly localized mode field within the core area at higher frequencies. Toluene has the lowest effective area and Hydrogen cyanide has the highest among the materials. The figure shows a minimum effective area of 6.624×10^{-8} m^2 and a maximum effective area of 9.403×10^{-8} m^2 for Toluene and Hydrogen cyanide respectively at 1.6 THz.

C. STUDY OF THE OPTICAL PROPERTIES

The numerical aperture (NA) defines the ability of an optical fiber to accept the light. Higher NA means higher angular ability to accept an incoming light. So, it is desirable to have high NA for a PCF based sensor. However very high NA is sometimes related to multimode fibers. As we have proposed a single-mode PCF in this paper, it is also not desirable for us to have ultra-high NA because it indicates the multi-modality of the PCF. Fig. 4(d) represents the numerical aperture of the sensor for the porosity variations for Hydrogen sulfide. It is designated from the figure that NA continuously decreases with the increment of the frequency. It is also exposed that higher porosity evinces slightly higher NA. The reason is that a higher porosity gives rise to the area of the hollow core which expands the angular acceptability of the incoming light to propagate into the fiber. The figure shows good NA of 0.3597, 0.3574 and 0.3545 for different porosities of 82.5%, 77.5% and 72.5% respectively at 1.6 THz. However, the maximum values of the numerical aperture are 0.4267, 0.4250, and 0.4232 for the porosities of 82.5%, 77.5%, and 72.5% respectively at 1.2 THz.

Birefringence of a fiber is the absolute value of the difference between the refractive index of the orthogonal polarization modes. For sensing applications, a higher value of birefringence is suitable for maintaining the polarization state. By using an asymmetric structure for our proposed design, we have obtained high birefringence of the order 10^{-3} for the five different industrial chemicals since the asymmetrical structure can preserve the polarization state when the light interacts with chemical liquids. Fig. 5(a) illustrates the characteristics of birefringence concerning frequency for different analytes. It is observed that Hydrogen cyanide has the highest average birefringence among the analytes because it has the lowest refractive index among them that offers greater refractive index difference of the orthogonal polarization modes. The slope of the birefringence curve changes for the lower index analytes. The maximum birefringence of 0.004169 and minimum birefringence of 0.003338 have been observed at 1.6 THz for hydrogen cyanide and toluene respectively.

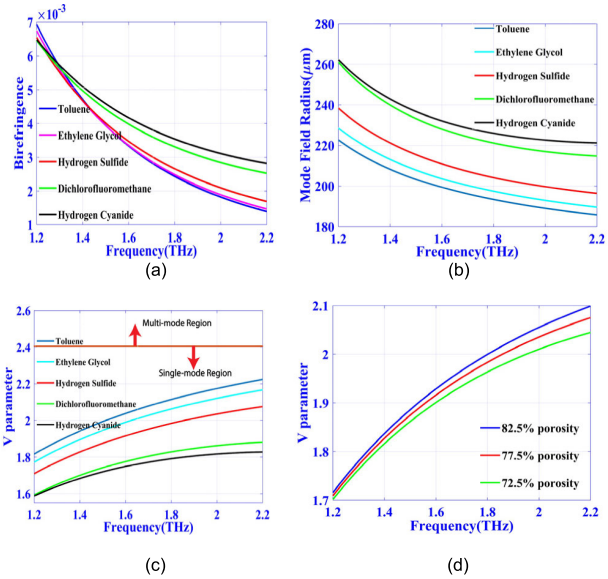

FIGURE 5. Illustration of optical characteristics of the proposed sensor: (a) birefringence (b) mode field radius (c) V parameter for different chemical analytes and (d) V parameter variations with respect to porosity changes.

Mode field radius is a vital parameter for determining the efficiency and sensitivity of a sensor as the splice loss can be minimized by reducing the difference between the MFR of a PCF and the core radius of an SMF, which is to be spliced with the waveguide. The radius of an equivalent circular area with respect to the formed core modal area figuratively gives the MFR. The MFR of 199.4 μm, 203.8 μm, 211 μm, 228.2 μm and 232.2 μm has been found for toluene, ethylene glycol, hydrogen sulfide, dichlorofluoromethane and hydrogen cyanide respectively at 1.6 THz. From Fig. 5(b), it can be observed that if the MFR of SMF lies between 180-265 μm range, the splice loss becomes negligibly small which will help to obtain viable output optical signal without attenuation.

Fig. 5(c) depicts the variation of the V parameter with frequency. It is observed that the values of the V parameter remain below 2.405 which indicates that the proposed PCF is a single-mode fiber. The maximum V parameters of 2.224, 2.167, 2.075, 1.881 and 1.827 are found for toluene, ethylene glycol, hydrogen sulfide, dichlorofluoromethane and hydrogen cyanide respectively at 2.2 THz. The single-mode behavior is desired as the total optical energy traverses through that fundamental mode. This effectively eliminates the undesired inter-modal dispersive properties. Fig. 5(d) shows V parameter values with different core porosities as a function of frequency in THz regime. The V parameter values are of 1.929, 1.916 and 1.901 for the porosities of 82.5%, 77.5% and 72.5% respectively at 1.6 THz. It is clear that the V parameter increases with the increment of porosity. Increasing porosity means increment in the area of the core which eases the angular acceptance of the incoming light. An increase in the angular acceptance of the light gives rise to the NA. The V parameter is directly proportional to the NA. So, the V parameter increases with the increment of porosities. Another reason for the increment in V parameter is that the core radius also increases with the escalation of porosity, As the V parameter is also directly proportional to the core radius it increases with the increment of porosity. Fig. 6 shows the variation of beam divergence with the frequency. Beam divergence is directly proportional to the wavelength of the light. When the incident light is of high intensity, the energy of the light is high which implies that the frequency is also high. As the frequency has an inversely proportional relationship with wavelength, this implies that increasing the frequency lowers the beam divergence as depicted in the figure. A lower value of the beam divergence from the beam waist is desirable. The beam divergences for this sensor are from 16.66° to 14.42° for toluene to hydrogen cyanide respectively.

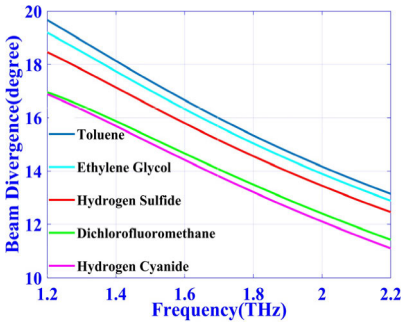

FIGURE 6. Beam divergence with respect to frequency for different chemical analytes.

D. COMPARATIVE ANALYSIS

Table 1 provides a comparison of characteristics with the designed PCF sensor with recently published PCF sensors in the THz regime. It is observed that, at 1.6 THz our proposed sensor displays higher relative sensitivity, lower EML, negligible confinement loss, and lower bending loss. From the comparison, it is evident that our proposed design has the highest relative sensitivity to the best of our knowledge. In addition to this, the index guided rectangular core of our design ensures very high confinement of light in the core. Material absorption losses are significantly reduced. Also, the bending attenuation is studied as well, which has not been frequently conducted in other studies. The structure unveils a significantly low bending loss in the operating region. From table 1, it is observed that the EML is higher for our sensor than that of [19] and [24]. In ref. [19], the authors proposed a PCF based sensor where EML is of 0.0008cm^{-1} at 2.2 THz frequency. They used much higher refractive indexed analytes than us. Higher refractive indexed analytes usually show lower EML value. Moreover, the width of TOPAS around the channel in [19] is much smaller compared to our sensor which can make the sensor difficult to fabricate. In ref. [24], the authors proposed a PCF based sensor where EML is of 0.0035cm^{-1} at 1.4THz. They used a hollow core rectangular shaped analyte channel where the width and height were of 500μm and 390μm respectively whereas the width and height of our analyte channel are of 240.6μm and 360.8μm. It is evident that authors in ref. [24] used larger analyte channel area than us. Larger area of the analyte channel helps to decrease the EML as most of the incident light can propagate through the analyte channel. However, it is possible to further decrease the EML for our sensor by increasing the height (H) and width (W) of the rectangular analyte channel. Fig. 7 shows EML curves for Toluene and H_2S for different heights and widths of the channel. It is evident from the figure that if we increase the height and width of the channel, the EML continuously decreases. The effective material loss is of 0.0044cm^{-1} for Toluene for the height and width of 375.8μm and 250.6μm respectively at 1.6THz. We have here increased the height and width by 15μm and 10μm respectively from the optimum value. After further increment, the effective material loss is found 0.0023cm^{-1} for Toluene for the height and width of 390.8μm and 260.6μm respectively at 1.6THz which is lower than that of [24]. We have intentionally kept our height and width lower to have more TOPAS around the channel that can make the design feasible to fabricate and give more rigidity to the waveguide. Moreover, using higher value of height and width of the channel effectively reduces the contrast of relative sensitivity among the chemicals in a particular frequency which is not good for sensing purpose.

The effective material loss (EML) is evaluated by the ratio of the field component passing through Topas and the overall fiber transverse section. It includes the absorption loss and the refractive index of Topas. It is obvious that maximum portion of the incident light passes through the core region. And the core region comprises of the analyte and the rectangular Topas channel framework. The amount of field components for different analytes can never be exactly equal to each other. Though the analytes are assumed lossless, the amount of field component passing through them is sheerly dependent on the respective analytes. This can be better analyzed in terms of spot size or the mode field radius. It can be observed

TABLE 1. Comparison among recently published PCF sensors in THz regime and our proposed sensor.

Ref	Geometry (core)	Optimum Frequency (THz)	Relative Sensitivity (%)	Effective Material Loss (cm^{-1})	Confinement loss	Birefringence	Bending loss
[23]	Porous circular	1	-	0.01944	10^{-6} dB/cm (approx.)	10^{-5} (approx.)	10^{-6} dB/cm (approx.)
[24]	Hollow core (rectangular)	1.4	96.8	0.0035	6.95×10^{-14} cm^{-1}	0.0155	-
[16]	Elliptical shaped	1.8	77.5	0.031	5.15×10^{-8} cm^{-1}	0.009	4.09×10^{-8} cm^{-1}
[25]	Hollow core (rectangular)	1.7	89	0.028	1.15×10^{-9} dB/cm	0.007	-
[14]	Hollow core (rectangular)	1.8	94.4	0.00859	1.71×10^{-14} cm^{-1}	0.00682	-
[26]	Sectored square	1	90±1	0.009	0.0004 cm^{-1}	-	-
[19]	Hollow core (octagonal)	2.2	98.75	0.0008	3.14×10^{-20} cm^{-1}	-	-
Proposed sensor	Hollow core (rectangular)	1.6	99.73	0.007	3.2×10^{-11} dB/m	0.0042	2.61×10^{-12} dB/m

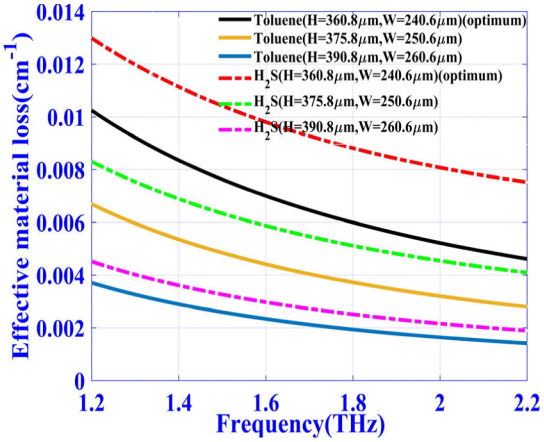

FIGURE 7. EML curves for Toluene and H2S for different heights and widths of the analyte channel.

from Fig. 5(b) and Fig. 4(c) of the manuscript that higher RI analytes have lower mode field radius and effective area. And for lower analyte RI, the mode field radius and the effective area is higher. From figure 3(d) it can be observed that, analytes with higher RI have lower EML and vice-versa. So, the argument is quite compelling that if the effective area and the spot size is high, then the EML is also high. The reason for that is also obvious. Higher effective area and spot size means that the portion of the field component passing through the Topas channel walls will also be high. Hence, the waveguide will undergo more EML. Thus, the EML has to differ for different analytes and they can never be the same.

In our previous work, SPR based optical sensor for a broad detection range has been proposed [27]. A high birefringence PCF for sensing purpose has also been reported [28]. Recently, a Fiber Bragg Grating based pressure sensor has been designed, tested and fabricated [29]. With the technological advancement THz propagation based optical sensors are now showing good promise to be fabricated as well.

IV. CONCLUSION

A rectangular-shaped hollow-core THz waveguide with four segmented air cladding is presented and anatomized in this paper for different toxic industrial compounds detection. Simulation results have disclosed and offered ultra-high relative sensitivity of 99.73%, 98.85%, 97.22%, 93.02% and 89.56% for Toluene, Ethylene glycol, Hydrogen sulfide, Dichlorofluoromethane and Hydrogen cyanide respectively at 1.6 THz. The sensor has exhibited ultra-low effective material loss of 0.007 cm^{-1} for Toluene at 1.6 THz. Confinement loss and bending loss are of the order 10^{-11} (dB/m) and 10^{-12} (dB/m) for Hydrogen sulfide and Ethylene glycol respectively. The values of V parameter for all compounds are in between 1.586 and 2.224 which confirms that the sensor supports single-mode propagation. The sensor shows a high birefringence of the order 10^{-3} for all the selected compounds. The paper has also tried to deliver an idea about the splice loss by showing the mode field radius of the fiber for all the chemicals. Our proposed sensor also shows a good and balanced numerical aperture of 0.36 at 1.6 THz for Hydrogen sulfide which ensures fine acceptability of the incoming light. Other important optical properties such as beam divergence and effective area have been studied, which unveil a very good serviceability of the sensor. The structural design of the sensor indicates its practicability for fabrication

with the existing technology. The designed sensor shows good promise for detecting toxic industrial chemicals as well as other environmental pollutants.

REFERENCES

[1] K. Ahmed, S. Chowdhury, B. K. Paul, M. S. Islam, S. Sen, and M. I. S. I. Asaduzzaman, "Ultrahigh birefringence, ultralow material loss porous core single-mode fiber for terahertz wave guidance," *Appl. Opt.*, vol. 56, no. 12, pp. 3477–3483, Apr. 2017.

[2] M. S. Islam, J. Sultana, K. Ahmed, M. R. Islam, A. Dinovitser, B. W.-H. Ng, and D. Abbott, "A novel approach for spectroscopic chemical identification using photonic crystal fiber in the terahertz regime," *IEEE Sensors J.*, vol. 18, no. 2, pp. 575–582, Jan. 2018.

[3] M. Nagel, P. H. Bolivar, M. Brucherseifer, H. Kurz, A. Bosserhoff, and R. Buttner, "Integrated THz technology for label-free genetic diagnostics," *Appl. Phys. Lett.*, vol. 80, no. 1, pp. 154–156, Jan. 2002.

[4] A. G. Markelz, A. Roitberg, and E. J. Heilweil, "Pulsed terahertz spectroscopy of DNA, bovine serum albumin and collagen between 0.1 and 2.0 THz," *Chem. Phys. Lett.*, vol. 320, nos. 1–2, pp. 42–48, Mar. 2000.

[5] B. M. Fischer, M. Hoffmann, H. Helm, R. Wilk, F. Rutz, T. Kleine-Ostmann, M. Koch, and P. U. Jepsen, "Terahertz time-domain spectroscopy and imaging of artificial RNA," *Opt. Exp.*, vol. 13, no. 14, pp. 5205–5215, Jul. 2005.

[6] V. Wallace, A. Fitzgerald, S. Shankar, N. Flanagan, R. Pye, J. Cluff, and D. Arnone, "Dermatological surgery and lasers terahertz pulsed imaging of basal cell carcinoma *ex vivo* and *in vivo*," *Brit. J. Dermatol.*, vol. 151, no. 2, pp. 424–432, 2004.

[7] K. Kawase, Y. Ogawa, Y. Watanabe, and H. Inoue, "Non-destructive terahertz imaging of illicit drugs using spectral fingerprints," *Opt. Exp.*, vol. 11, no. 20, pp. 2549–2554, Oct. 2003.

[8] H. Liu, Y. Chen, G. Bastiaans, and X. Zhang, "Detection and identification of explosive RDX by THz diffuse reflection spectroscopy," *Opt. Exp.*, vol. 14, no. 1, pp. 415–423, Jan. 2006.

[9] S. Biswas, R. Arfin, A. Habib, S. Amir, Z. Zahir, M. Islam, and M. Hussain, "A modified design of a hexagonal circular photonic crystal fiber with large negative dispersion properties and ultrahigh birefringence for optical broadband communication," *Photonics*, vol. 6, no. 1, p. 19, Feb. 2019.

[10] H. Talukder, M. I. A. Isti, S. Nuzhat, and S. K. Biswas, "Ultra-high negative dispersion based single mode highly nonlinear bored core photonic crystal fiber (HNL-BCPCF): Design and numerical analysis," *Brazilian J. Phys.*, vol. 50, no. 3, pp. 263–271, Jun. 2020.

[11] M. I. A. Isti, H. Talukder, S. M. R. Islam, S. Nuzhat, A. S. M. S. Hosen, G. H. Cho, and S. K. Biswas, "Asymmetrical D-channel photonic crystal fiber-based plasmonic sensor using the wavelength interrogation and lower birefringence peak method," *Results Phys.*, vol. 19, Dec. 2020, Art. no. 103372.

[12] M. A. Habib, M. S. Anower, and M. R. Hasan, "Highly birefringent and low effective material loss microstructure fiber for THz wave guidance," *Opt. Commun.*, vol. 423, pp. 140–144, Sep. 2018.

[13] R. Islam, M. S. Habib, G. K. M. Hasanuzzaman, S. Rana, M. A. Sadath, and C. Markos, "A novel low-loss diamond-core porous fiber for polarization maintaining terahertz transmission," *IEEE Photon. Technol. Lett.*, vol. 28, no. 14, pp. 1537–1540, Jul. 15, 2016.

[14] M. B. Hossain, E. Podder, A. A.-M. Bulbul, and H. S. Mondal, "Bane chemicals detection through photonic crystal fiber in THz regime," *Opt. Fiber Technol.*, vol. 54, Jan. 2020, Art. no. 102102.

[15] M. S. Islam, J. Sultana, J. Atai, D. Abbott, S. Rana, and M. R. Islam, "Ultra low-loss hybrid core porous fiber for broadband applications," *Appl. Opt.*, vol. 56, no. 4, pp. 1232–1237, 2017.

[16] M. S. Islam, J. Sultana, A. Dinovitser, K. Ahmed, B. W.-H. Ng, and D. Abbott, "Sensing of toxic chemicals using polarized photonic crystal fiber in the terahertz regime," *Opt. Commun.*, vol. 426, pp. 341–347, Nov. 2018.

[17] H. Ebendorff-heidepriem, J. Schuppich, A. Dowler, L. Lima-marques, and T. M. Monro, "3D-printed extrusion dies: A versatile approach to optical material processing," *Opt. Mater. Exp.*, vol. 4, no. 8, pp. 1494–1504, Aug. 2014.

[18] S. Atakaramians, S. Afshar, H. Ebendorff-Heidepriem, M. Nagel, B. M. Fischer, D. Abbott, and T. M. Monro, "THz porous fibers: Design, fabrication and experimental characterization," *Opt. Exp.*, vol. 17, no. 16, pp. 14053–14062, Aug. 2009.

[19] M. M. Rahman, F. A. Mou, M. I. H. Bhuiyan, and M. R. Islam, "Photonic crystal fiber based terahertz sensor for cholesterol detection in human blood and liquid foodstuffs," *Sens. Bio-Sensing Res.*, vol. 29, Aug. 2020, Art. no. 100356.

[20] B. Paul, M. Haque, K. Ahmed, and S. Sen, "A novel hexahedron photonic crystal fiber in terahertz propagation: Design and analysis," *Photonics*, vol. 6, no. 1, p. 32, Mar. 2019.

[21] S. Islam, B. Kumar, and K. Ahmed, "Liquid-infiltrated photonic crystal fiber for sensing purpose: Design and analysis," *Alexandria Eng. J.*, vol. 57, no. 3, pp. 1459–1466, Sep. 2018.

[22] R. Hasan, S. Anower, A. Islam, and S. M. A. Razzak, "Polarization-maintaining low-loss porous-core spiral photonic crystal fiber for terahertz wave guidance," *Appl. Opt.*, vol. 55, no. 15, pp. 4145–4152, May 2016.

[23] S. Ali, N. Ahmed, S. Aljunid, and B. Ahmad, "Hybrid porous core low loss dispersion flattened fiber for THz propagation," *Photon. Nanostruct.-Fundam. Appl.*, vol. 22, pp. 18–23, Nov. 2016.

[24] M. S. Islam, J. Sultana, A. A. Rifat, A. Dinovitser, B. W.-H. Ng, and D. Abbott, "Terahertz sensing in a hollow core photonic crystal fiber," *IEEE Sensors J.*, vol. 18, no. 10, pp. 4073–4080, Mar. 2018.

[25] M. A. Habib, M. S. Anower, L. F. Abdulrazak, and M. S. Reza, "Hollow core photonic crystal fiber for chemical identification in terahertz regime," *Opt. Fiber Technol.*, vol. 52, Nov. 2019, Art. no. 101933.

[26] F. Akter, M. Rahman, M. Rakibul, M. Imamul, and H. Bhuiyan, "Research development of a photonic crystal fiber for THz wave guidance and environmental pollutants detection," *Sens. Bio-Sensing Res.*, vol. 29, Mar. 2020, Art. no. 100346.

[27] M. H. K. Anik, M. I. A. Isti, S. M. R. Islam, S. Mahmud, H. Talukder, M. J. Piran, S. K. Biswas, and K.-S. Kwak, "Milled microchannel-assisted open D-channel photonic crystal fiber plasmonic biosensor," *IEEE Access*, vol. 9, pp. 2924–2933, Dec. 2021.

[28] M. S. Islam, C. M. B. Cordeiro, J. Sultana, R. A. Aoni, S. Feng, R. Ahmed, M. Dorraki, A. Dinovitser, B. W.-H. Ng, and D. Abbott, "A Hi-Bi ultra-sensitive surface plasmon resonance fiber sensor," *IEEE Access*, vol. 7, pp. 79085–79094, Jun. 2019.

[29] C. Hong, Y. Zhang, and L. Borana, "Design, fabrication and testing of a 3D printed FBG pressure sensor," *IEEE Access*, vol. 7, pp. 38577–38583, Mar. 2019.

M. HUSSAYEEN KHAN ANIK is currently pursuing the B.Sc. degree with the Faculty of Electrical and Electronic Engineering, Shahjalal University of Science and Technology. He is currently doing his research program in photonics and plasmonics with the Shahjalal University of Science and Technology. His research interests include fiber optics, photonics, plasmonics, and optical biosensors.

S. M. RIAZUL ISLAM (Member, IEEE) was affiliated with Memorial University, Canada, as a Postdoctoral Fellow. Before that, he was with the University of Dhaka, Bangladesh, as an Assistant Professor and a Lecturer with the Department of Electrical and Electronics Engineering. He also worked with the Samsung Research and Development Institute Bangladesh as a Chief Engineer with the Department of Solution Laboratory for Advanced Research. He is currently an Assistant Professor with the Department of Computer Science and Engineering, Sejong University, South Korea. Prior to Sejong University, he worked with the Wireless Communications Research Center, Inha University, South Korea, as a Postdoctoral Fellow. His research interests include wireless communications, the Internet of Things, and applied artificial intelligence.

SHOVASIS KUMAR BISWAS (Member, IEEE) received the B.Sc. and M.Sc. degrees in applied physics, electronics and communication engineering from the University of Dhaka, Dhaka, Bangladesh, in 2011 and 2013, respectively, and the M.A.Sc. degree in electrical and computer engineering from McMaster University, Canada, in 2016. He is currently working as a Lecturer with the Department of Electrical and Electronic Engineering, Independent University at Bangladesh, Dhaka. He has published several articles in journals as well as in the proceedings of IEEE flagship/portfolio conferences. His research interests include nanophotonics, plasmonics, optical biosensor, photonic crystal fiber, and optical fiber communication.

M. IFAZ AHMAD ISTI received the B.Sc. degree in electrical and electronic engineering from the Shahjalal University of Science and Technology (SUST), Sylhet, Bangladesh, in 2020. He is currently working as a Research Assistant in optics and photonics with the Department of Electrical Engineering, SUST. He is also a Former Secretary of IEEE, Student Branch, SUST. His research interests include fiber optics, photonic crystals, plasmonics, and optical biosensors.

MOHONA DAS GUPTA received the B.Sc. degree in electrical and electronic engineering from the Shahjalal University of Science and Technology, Sylhet, Bangladesh, in 2020. She is currently a Former Vice-Chairman of IEEE (WIE), Student Branch, SUST. Her research interests include fiber optics, photonics, plasmonics, and optical biosensors.

MD. JALIL PIRAN (Senior Member, IEEE) received the Ph.D. degree in electronics and radio engineering from Kyung Hee University, South Korea, in 2016. He was a Postdoctoral Research Fellow in resource management and quality of experience in 5G cellular networks and the Internet of Things with the Networking Laboratory, Kyung Hee University. He is currently an Assistant Professor with the Department of Computer Science and Engineering, Sejong University, Seoul, South Korea. He has published substantial number of technical articles in well-known international journals and conferences in research fields of ''5G and 6G wireless communications, the Internet of Things (IoT), multimedia communication, cognitive radio networks, applied machine learning, security, and smart grid.'' In the worldwide communities, he has been an Active Member of Institute of Electrical and Electronics Engineering (IEEE), since 2010, an Active Delegate from South Korea in Moving Picture Experts Group (MPEG), since 2013, and an Active Member of the International Association of Advanced Materials (IAAM), since 2017. He received the IAAM Scientist Medal, in 2017, for notable and outstanding research in the field of New Age Technology and Innovation, Stockholm, Sweden. He has been recognized as the ''Outstanding Emerging Researcher'' by the Iranian Ministry of Science, Technology, and Research, in 2017, and his Ph.D. dissertation has been selected as the ''Dissertation of the Year 2016'' by the Iranian Academic Center for Education, Culture, and Research, in electrical and communications engineering.

KYUNG-SUP KWAK (Life Senior Member, IEEE) received the B.S. degree from Inha University, Incheon, South Korea, in 1977, the M.S. degree from the University of Southern California, in 1981, and the Ph.D. degree from the University of California at San Diego, in 1988, under the Inha University Fellowship and the Korea Electric Association Abroad Scholarship Grants. He worked with Hughes Network System, San Diego, CA, USA, and the IBM Network Research Center, Research Triangle Park, NC, USA, from 1988 to 1990. Since 1990, he has been with Inha University as the Inha Fellow Professor. He is currently the Inha Hanlim Professor and the Director of the UWB Wireless Communications Research Center, South Korea. His research interests include multiple access communication systems, mobile communication systems, UWB radio systems and ad-hoc networks, and high-performance wireless internet. He is a member of IEICE, KICS, and KIEE.

HRITESHWAR TALUKDER (Member, IEEE) received the B.Sc. (Engg.) degree in electrical and electronic engineering from the Shahjalal University of Science and Technology, Bangladesh, in 2017. He is currently working as a Lecturer with the Shahjalal University of Science and Technology. His research interests include nonlinear optics, nanophotonics, plasmonics, optical biosensor, photonic crystal fiber, and optical fiber communication.